



ELSEVIER

Contents lists available at SciVerse ScienceDirect

Journal of Physics and Chemistry of Solids

journal homepage: www.elsevier.com/locate/jpcs

Synthesis of organic phenothiazine-based molecular glasses and effect of racemic/homochiral aliphatic chain on near-infrared photorefractive property

Yingliang Liu, Ryushi Fujimura, Kazuki Ishida, Nobuhiro Oya, Naoko Yoshie, Tsutomu Shimura*, Kazuo Kuroda

Institute of Industrial Science, The University of Tokyo, 4-6-1 Komaba, Meguro-ku, Tokyo 153-8505, Japan

ARTICLE INFO

Article history:

Received 26 November 2011

Received in revised form

16 February 2012

Accepted 19 April 2012

Available online 9 May 2012

Keywords:

A. Amorphous materials

A. Optical materials

A. Organic compounds

A. Thin films

B. Chemical synthesis

ABSTRACT

Organic near-infrared photorefractive molecular glasses with a phenothiazine moiety are designed and synthesized through the introduction of linear, racemic/homochiral asymmetrically branched aliphatic chains into photorefractive chromophore as an auxiliary group. The compounds are characterized with ¹H-NMR, IR, FAB-MS, UV-vis, TG, DSC, etc. The effect of different aliphatic chains on the absorption and thermal properties is investigated in detail. The molar absorption coefficient at the absorption maximum wavelength showed that the homochiral asymmetrically branched aliphatic chain has a strong hypochromic effect in the dilute solution when it is introduced into photorefractive chromophore. The DSC measurement indicated that the introduction of asymmetrically branched aliphatic chain is the key issue to design organic molecular glasses whether it is racemic or homochiral. The effect of racemic/homochiral asymmetrically branched aliphatic groups on photorefractive property is investigated carefully with poly(*N*-vinylcarbazole) (PVK) as a photoconductor and with (2,4,7-trinitro-9-fluorenylidene) malononitrile (TNFM) as a photosensitizer. The results suggested that the racemic group is more beneficial to the improvement of photorefractive performance than the homochiral when the homochiral cannot induce rigid photorefractive chromophore to be much more ordered.

© 2012 Elsevier Ltd. All rights reserved.

1. Introduction

Organic molecular glass has recently attracted much attention due to its property tunability through the modification of chemical structure and the thermal/optical stability in film, which is a key issue for practical application of organic optoelectronic devices, such as organic photorefractive devices (OPRs) [1–5], organic light-emitting diodes (OLEDs) [6–9], organic photovoltaic cells (OPVs) [10,11], organic field-effect transistors (OFETs) [12,13], etc. Since especially, organic glasses for photorefractive materials were first reported by Lundquist et al. [14], organic photorefractive glasses have made much progress not only in the synthesis of materials [15–17] but also in the physic mechanism of devices [18–23]. Simultaneously, the photorefractive response wavelength is also extended to the near-infrared region [24]. In general, organic molecular glasses (also called as monolithic molecules) are referred to as a class of organic compounds being able to keep an amorphous state without any dopant, which is different from the organic composite glass. In principle, the

dopant in organic composite materials can block the crystallizing of crystalline compounds in film, temporarily affording the uniform film. With time passing by, the crystalline compound still tends to form a crystal microparticle, which is a crucial factor of the instability for optoelectronic devices. However, organic molecular glasses will overcome this disadvantage extraordinarily keeping themselves in amorphous state. In this occasion, the solid film is optically uniform without light-scattering and transmission-attenuating. Therefore, organic photorefractive molecular glasses have become a prospective candidate for the practical application of photorefractive devices.

Notably, the optoelectronic properties are rarely investigated from organic chiral molecular glasses because it is very difficult for the enantiomerically pure compounds to form an amorphous phase state. Recently, chiral molecular glasses have been presented with one thiophene-based enantiopure helicene forming a rare chiral molecular glass while its chiroptical properties were enhanced [25]. The chirality effect on nonlinear optical properties has been studied extensively [26–35]. The chirality effect on photorefractive performance was also reported in organic photorefractive liquid crystal [36–39]. As one of the promising optoelectronic materials, organic photorefractive molecular glass is also scarcely investigated up to date without exception through

* Corresponding author. Tel.: +81 3 5452 6137; fax: +81 3 5452 6140.

E-mail addresses: shimura@iis.u-tokyo.ac.jp, liuylxn@sohu.com (T. Shimura).

the introduction of chiral group into the chromophore due to its more complicated mechanism although high-efficient erasable polarization gratings have been optically recorded in a molecular glass composed of azobenzene and chiral isosorbide moieties [40]. It is well known that charge-transfer complexes between donor and acceptor usually take a role of the photosensitizer, which is one of the important component in photorefractive composite film. When organic chiral molecular glass is applied as photorefractive chromophore, it is possible for chiral molecular glass to affect the photosensitive effect of the photosensitizer, i.e., charge-transfer complex between chiral molecular glass and other acceptors, which is generally (2,4,7-trinitro-9-fluorenylidene) malononitrile (TNFM), 2,4,7 trinitro-9-fluorenone (TNF) and so on. To the best of our knowledge, the investigation in point is not reported even if chiral charge-transfer complexes have been studied on several occasions [41–43].

In this paper, organic near-infrared photorefractive molecular glasses with a phenothiazine moiety are designed and synthesized through the introduction of linear, racemic/homochiral asymmetrically branched aliphatic chains into photorefractive chromophore as an auxiliary group. The compounds are characterized with $^1\text{H-NMR}$, IR, FAB-MS, UV-vis, TG, DSC, etc. Especially, the effect of different aliphatic chains on absorption and thermal properties is investigated in detail, including linear, racemic/homochiral asymmetrically branched aliphatic chains. Additionally, the effect of racemic/homochiral asymmetrically branched aliphatic chains on photorefractive property is also measured carefully with the PVK as a photoconductive polymer and with TNFM as a photosensitizer.

2. Experimental section

2.1. Characterization and instruments

$^1\text{H-NMR}$ spectroscopy was recorded on JEOL JNM-AL400 using chloroform-*d* solution at room temperature. Infrared (IR) spectroscopy was measured using a JEOL WINSPEC100 spectrometer. The fast atom bombardment mass spectrometry (FAB-MS) was performed on JEOL JMS-600H mass spectrometer using 3-nitrobenzylalcohol as a matrix. The molecular weight of PVK was monitored by gel permeation chromatography (GPC) on Tosoh HLC 822 using the chloroform as an eluent (1 mL/min) at 40 °C and with the polystyrenes as calibration standards. Thermogravimetry (TG) was investigated on Thermo Plus TG 8120 at heating and cooling rates of 10 °C/min under N_2 atmosphere. Differential scanning calorimetry (DSC) was carried out with Perkin-Elmer Pyris I at heating and cooling rates of 10 °C/min under N_2 atmosphere. Ultraviolet-visible (UV-vis) spectra were

recorded using a cuvette of thickness 1 cm on a HITACHI U-3010 spectrophotometer. The transmittance spectra were performed *in-situ* with the photorefractive devices as a sample by an U-4000 spectrophotometer. The DPS-3001 laser diode with a laser wavelength of 780 nm from NIHON KAGAKU ENG Corp. was used during the photorefractive measurement. The electric field was applied on the photorefractive devices with HEOPS-5B6 high voltage amplifier as a high voltage power supply. The current of photorefractive devices was monitored with a KEITHLEY 6517A electrometer. The piezomirror was translated with a piezoelectric stage driven by low voltage PZT driver and TEKTRONIX AFG 3021 function generator. The shutter was controlled by SIGMA KOKI Σ -65L shutter controller. The total power of transmitted signals was monitored by identical NEW FOCUS 2033-M large-area photoreceivers and recorded by LeCroy LC 334AM 500 MHz oscilloscope.

2.2. Reagents and materials

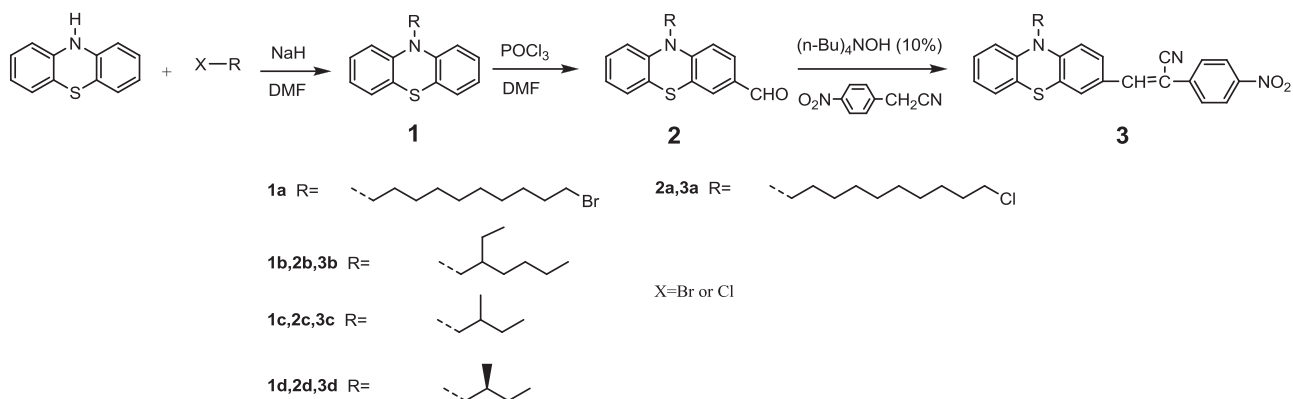
Phenothiazine, 1,10-dibromooctane, *p*-nitrophenylacetonitrile, (*n*-Bu) $_4$ NOH(10%), 1-bromo-2-ethylhexane, 1-chloro-2-methylbutane, poly(*N*-vinylcarbazole) (PVK), (2,4,7-trinitro-9-fluorenylidene) malononitrile (TNFM) were bought from Tokyo Chemical Industry (TCI) and (*S*)-(+)-1-bromo-2-methylbutane from Sigma-Aldrich. Other chemicals and solvents were purchased from Wako chemical company. All the chemicals were used without any purification. The filter with a pore size of 0.2 μm , which was built of polytetrafluoroethylene (PTFE) membrane with a polypropylene housing, was purchased from Whatman incorporation.

2.3. Synthesis

All the intermediates and target compounds are synthesized according to the synthetic route in Scheme 1. Basically, all the target compounds follow the same or similar synthetic procedure. First, different aliphatic chains are linked onto phenothiazine by alkylation reaction between phenothiazine and alkylhalide. Then, an aldehyde group is added to phenothiazine by Vilsmeier reaction of *N*-alkyl-phenothiazine. Finally, the acceptor is connected with phenothiazine by the below Knoevenagel reaction. The specific synthetic procedures are given.

2.3.1. General procedure for synthesis of compound 1

A typical procedure is given with compound **1a** as an example. Phenothiazine (3.0 g, 15 mmol) was completely dissolved in DMF (30 ml) and then NaH (1.2 g) was added. After the reaction was carried out in an ice bath under a vigorous stirring for half an hour, 1,10-dibromooctane (13.5 g, 45 mmol) was immediately added to the mixture. The reaction was sequentially going on at



Scheme 1. Synthetic route of phenothiazine-based compounds with different aliphatic chains.

room temperature for another 4 h. Finally, the mixture was poured into distilled water (600 ml), and extracted with *n*-hexane for three times (400 ml each). The extracting solution was dried with anhydrous magnesium sulfate overnight. After the magnesium sulfate was filtrated out, *n*-hexane was evaporated from the filtrate under reduced pressure. The crude product was purified by silica-gel column chromatography. When compounds **1b**, **1c**, **1d** were synthesized, alkane bromide was added with a excess of 20% instead of 200%.

Compound 1a: Chloroform was used as eluent (Rf value: 0.53). Compound **1a** was not identified and directly used in the next reaction.

Compound 1b: *n*-hexane was used as eluent (Rf value: 0.15). Compound **1b** was obtained as a buff viscous liquid in 59.8% yield. FAB-MS: $m/z=311.2$ [M]⁺. UV-vis (THF): $\lambda_{\max}=309$ nm. ¹H-NMR (400 MHz, Chloroform-*d*, δ): 0.86 (m, 6H, CH₃ × 2), 1.26 (m, 4H, CH₂ × 2), 1.36–1.47 (m, 4H, CH₂ × 2), 1.93 (m, 1H, CH), 3.72 (b, 2H, CH₂N), 6.88 (d, $J=8.8$ Hz, 2H, PTzH × 2), 6.90 (b, 2H, PTzH × 2), 7.14 (t, $J=7.6$ Hz, 4H, PTzH × 4). IR (KBr, ν/cm^{-1}): 3063 (CH on the phenothiazine ring), 2957, 2926 (ν_{as} , CH), 2856 (ν_{s} , CH), 1593, 1568, 1485 (benzene ring), 1456 (CH₂), 1380 (CH₃), 1329, 1285 (C–N), 1250, 1221 (C–CH₃), 748 (R(CH₂)₄–C).

Compound 1c: Rf value: 0.15 (*n*-hexane). Compound **1c** was obtained as a viscous liquid in 16.0% yield. FAB-MS: $m/z=269.2$ [M]⁺. UV-vis (THF): $\lambda_{\max}=308$ nm. ¹H-NMR (400 MHz, Chloroform-*d*, δ): 0.90 (t, $J=7.2$ Hz, 3H, CH₃), 0.96 (d, $J=7.2$ Hz, 3H, CH₃), 1.22 (m, 1H, CH), 1.56 (m, 1H, CH), 2.02 (m, 1H, CH), 3.59 (b, 1H, CH), 3.77 (b, 1H, CH), 6.85 (d, $J=7.6$ Hz, 2H, PTzH × 2), 6.90 (b, 2H, PTzH × 2), 7.14 (t, $J=7.2$ Hz, 2H, PTzH × 2), 7.16 (t, $J=6.8$ Hz, 2H, PTzH × 2). IR (KBr, ν/cm^{-1}): 3063 (CH on the phenothiazine ring), 2959, 2926 (ν_{as} , CH), 2872 (ν_{s} , CH), 1593, 1571, 1484, 1457 (benzene ring), 1249 (C–N), 1250, 1223 (C–CH₃), 748 (CH).

Compound 1d: Rf value: 0.21 (*n*-hexane). Compound **1d** was obtained as a buff viscous product in 57.7% yield. FAB-MS: $m/z=269.2$ [M]⁺. UV-vis (THF): $\lambda_{\max}=308$ nm. ¹H-NMR (400 MHz, Chloroform-*d*, δ): 0.91 (t, $J=7.2$ Hz, 3H, CH₃), 0.97 (d, $J=6.8$ Hz, 3H, CH₃), 1.23 (m, 1H, CH), 1.56 (m, 1H, CH), 2.02 (m, 1H, CH), 3.60 (b, 1H, CH), 3.78 (b, 1H, CH), 6.87 (d, $J=8.0$ Hz, 2H, PTzH × 2), 6.92 (b, 2H, PTzH × 2), 7.15 (t, $J=7.6$ Hz, 4H, PTzH × 4). IR (KBr, ν/cm^{-1}): 3063 (CH on the phenothiazine ring), 2959, 2926 (ν_{as} , CH), 2853 (ν_{s} , CH), 1593, 1570, 1485, 1456 (benzene ring), 1248 (C–N), 1248, 1223 (C–CH₃), 748 (CH).

2.3.2. General procedure for synthesis of compound 2

A typical procedure was given with compound **2a** as an example. Compound **1a** in the above step was all dissolved in DMF (30 ml) and cooled to 0 °C with an ice bath. Then, phosphoryl chloride (23.1 g, 150 mmol) was added dropwise to the mixture under a vigorous stirring. After that, the reactant was heated to 70 °C under the protection of N₂ for 4 h. The mixture was finally poured into distilled water (500 ml) and extracted with chloroform. The extracting solution was dried overnight with anhydrous magnesium sulfate. After magnesium sulfate was filtrated out, chloroform was removed under reduced pressure. The residue was dissolved in a minimal amount of chloroform and purified by silica-gel column chromatography using chloroform as an eluent.

Compound 2a: Rf value: 0.12 (chloroform). Compound **2a** was obtained as a yellow solid in 43.3% yield. FAB-MS: $m/z=401.2$ [M]⁺. UV-vis (THF): $\lambda_{\max}=379$ nm. ¹H-NMR (400 MHz, Chloroform-*d*, δ): 1.28 (m, 8H, (CH₂)₄), 1.43 (m, 4H, CH₂ × 2),

1.76 (p, $J=7.2$ Hz, 2H, CH₂), 1.82 (p, $J=7.2$ Hz, 2H, CH₂), 3.54 (t, $J=6.8$ Hz, 2H, CH₂Cl), 3.90 (t, $J=7.2$ Hz, 2H, CH₂N), 6.90 (d, $J=6.8$ Hz, 1H, PTzH), 6.92 (d, $J=8.0$ Hz, 1H, PTzH), 6.98 (t, $J=7.6$ Hz, 1H, PTzH), 7.12 (d, $J=7.6$ Hz, 1H, PTzH), 7.18 (t, $J=8.0$ Hz, 1H, PTzH), 7.59 (s, 1H, PTzH), 7.64 (d, $J=8.0$ Hz, 1H, PTzH), 9.80 (s, 1H, CHO). IR (KBr, ν/cm^{-1}): 2926 (ν_{as} , CH), 2853 (ν_{s} , CH), 2723 (CH on CHO), 1688 (C=O), 1597, 1572, 1556 (benzene ring), 1464 (CH₂), 1369, 1337, 1286 (C–N), 1250 (*m*-disubstitution on the benzene ring), 748 (R(CH₂)₄–C).

Compound 2b: Rf value: 0.42 (chloroform). Compound **2b** was obtained as a yellow liquid in 89.4% yield. FAB-MS: $m/z=339.1$ [M]⁺. UV-vis (THF): $\lambda_{\max}=377$ nm. ¹H-NMR (400 MHz, Chloroform-*d*, δ): 0.87 (m, 6H, CH₃ × 2), 1.26 (m, 4H, CH₂ × 2), 1.34–1.46 (m, 4H, CH₂ × 2), 1.92 (m, 1H, CH), 3.78 (d, $J=6.8$ Hz, 2H, CH₂N), 6.92 (d, $J=8.0$ Hz, 1H, PTzH), 6.94 (d, $J=8.4$ Hz, 1H, PTzH), 6.98 (t, $J=7.6$ Hz, 1H, PTzH), 7.14 (d, $J=8.0$ Hz, 1H, PTzH), 7.17 (t, $J=8.0$ Hz, 1H, PTzH), 7.62 (s, 1H, PTzH), 7.66 (d, $J=8.4$ Hz, 1H, PTzH), 9.80 (s, 1H, CHO). IR (KBr, ν/cm^{-1}): 3059 (CH on the phenothiazine ring), 2957, 2926 (ν_{as} , CH), 2856 (ν_{s} , CH), 2723 (CH on CHO), 1688 (C=O), 1597, 1572, 1493 (benzene ring), 1460 (CH₂), 1378 (CH₃), 1348 (CHR₃), 1333, 1310, 1286 (C–N), 1250, 1225 (C–CH₃), 746 (R(CH₂)₄–C).

Compound 2c: Rf value: 0.29 (chloroform). Compound **2c** was obtained as a yellow liquid in 91.3% yield. FAB-MS: $m/z=297.1$ [M]⁺. UV-vis (THF): $\lambda_{\max}=376$ nm. ¹H-NMR (400 MHz, Chloroform-*d*, δ): 0.91 (t, $J=7.2$ Hz, 3H, CH₃), 0.96 (d, $J=6.8$ Hz, 3H, CH₃), 1.24 (m, 1H, CH), 1.56 (m, 1H, CH), 2.00 (m, 1H, CH), 3.66 (p, $J=8.0$ Hz, 1H, CH), 3.83 (p, $J=6.4$ Hz, 1H, CH), 6.89 (d, $J=8.0$ Hz, 1H, PTzH), 6.94 (d, $J=8.0$ Hz, 1H, PTzH), 6.98 (t, $J=7.2$ Hz, 1H, PTzH), 7.14 (d, $J=8.0$ Hz, 1H, PTzH), 7.18 (t, $J=8.0$ Hz, 1H, PTzH), 7.62 (s, 1H, PTzH), 7.64 (d, $J=7.2$ Hz, 1H, PTzH), 9.80 (s, 1H, CHO). IR (KBr, ν/cm^{-1}): 2960, 2928 (ν_{as} , CH), 2873 (ν_{s} , CH), 2725 (CH on CHO), 1684 (C=O), 1596, 1572, 1493 (benzene ring), 1375 (CH₃), 1345 (CHR₃), 1310, 1288 (C–N), 1251, 1226 (C–CH₃), 747 (CH).

Compound 2d: Rf value: 0.50 (chloroform). Compound **2d** was obtained as a yellow liquid in 91.0% yield. FAB-MS: $m/z=297.3$ [M]⁺. UV-vis (THF): $\lambda_{\max}=377$ nm. ¹H-NMR (400 MHz, Chloroform-*d*, δ): 0.91 (t, $J=7.6$ Hz, 3H, CH₃), 0.97 (d, $J=6.8$ Hz, 3H, CH₃), 1.23 (m, 1H, CH), 1.56 (m, 1H, CH), 2.00 (m, 1H, CH), 3.65 (p, $J=8.0$ Hz, 1H, CH), 3.82 (p, $J=6.8$ Hz, 1H, CH), 6.91 (d, $J=9.6$ Hz, 1H, PTzH), 6.93 (d, $J=8.4$ Hz, 1H, PTzH), 6.98 (t, $J=6.8$ Hz, 1H, PTzH), 7.14 (d, $J=7.6$ Hz, 1H, PTzH), 7.17 (t, $J=8.0$ Hz, 1H, PTzH), 7.61 (s, 1H, PTzH), 7.64 (d, $J=8.0$ Hz, 1H, PTzH), 9.80 (s, 1H, CHO). IR (KBr, ν/cm^{-1}): 3059 (CH on the phenothiazine ring), 2961, 2926 (ν_{as} , CH), 2855 (ν_{s} , CH), 2723 (CH on CHO), 1686 (C=O), 1597, 1572, 1491, 1462 (benzene ring), 1375 (CH₃), 1344 (CHR₃), 1310, 1288 (C–N), 1252, 1198 (C–CH₃), 748 (CH).

2.3.3. General procedure for synthesis of compound 3

A typical procedure was given with compound **3a** as an example. (*n*-Bu)₄NOH (10%, 1 ml) was dropwise added to a stirred solution of compound **2** (2.21 g, 5.5 mmol) and *p*-nitrophenylacetonitrile (0.89 g, 5.5 mmol) in THF (10 ml). Then, the mixture was heated to 60 °C under the protection of N₂ atmosphere. After the reaction was carried out for 5 h, the mixture was cooled to room temperature and precipitated with distilled water (600 ml). The viscous precipitate with a purple black was dissolved in chloroform and dried overnight with anhydrous magnesium sulfate. After filtration, most of the solvent was evaporated under a reduced pressure. A small quantity of chloroform was reserved in order to dissolve the product. Finally, the crude product was

purified by silica-gel column chromatography using chloroform as an eluent.

Compound 3a: Rf value: 0.55 (chloroform). Compound **3a** was obtained as a red purple powder in 53.3% yield. FAB-MS: $m/z=545.3$ $[M]^+$. UV-vis (THF): $\lambda_{\max}=458$ nm. $^1\text{H-NMR}$ (400 MHz, Chloroform- d , δ): 1.28 (m, 8H, $(\text{CH}_2)_4$), 1.42 (m, 4H, $\text{CH}_2 \times 2$), 1.75 (p, $J=7.2$ Hz, 2H, CH_2), 1.82 (p, $J=7.2$ Hz, 2H, CH_2), 3.52 (t, $J=6.8$ Hz, 2H, CH_2Cl), 3.88 (t, $J=7.2$ Hz, 2H, CH_2N), 6.87 (d, $J=8.4$ Hz, 1H, PTzH), 6.90 (d, $J=8.8$ Hz, 1H, PTzH), 6.96 (t, $J=7.2$ Hz, 1H, PTzH), 7.10 (d, $J=7.2$ Hz, 1H, PTzH), 7.17 (t, $J=8.0$ Hz, 1H, PTzH), 7.49 (s, 1H, PTzH), 7.61 (s, 1H, =CH), 7.78 (d, $J=8.8$ Hz, 2H, ArH), 7.85 (d, $J=8.8$ Hz, 1H, PTzH), 8.27 (d, $J=8.8$ Hz, 2H, ArH). IR (KBr, ν/cm^{-1}): 2924 (ν_{as} , CH), 2851 (ν_{s} , CH), 2212 (CN), 1604, 1564, 1516 (benzene ring), 1470 (CH_2), 1399, 1338 (C–N), 1364 (NO_2), 850 (p -disubstitution on the benzene ring).

Compound 3b: Rf value: 0.57 (chloroform). Compound **3b** was obtained as a wine-colored powder in 50.3% yield. FAB-MS: $m/z=483.2$ $[M]^+$. UV-vis (THF): $\lambda_{\max}=455$ nm. $^1\text{H-NMR}$ (400 MHz, Chloroform- d , δ): 0.88 (m, 6H, $\text{CH}_3 \times 2$), 1.28 (m, 4H, $\text{CH}_2 \times 2$), 1.38–1.49 (m, 4H, $\text{CH}_2 \times 2$), 1.94 (m, 1H, CH), 3.78 (d, $J=6.8$ Hz, 2H, CH_2N), 6.92 (d, $J=8.4$ Hz, 1H, PTzH), 6.94 (d, $J=8.4$ Hz, 1H, PTzH), 6.98 (t, $J=7.3$ Hz, 1H, PTzH), 7.14 (d, $J=8.0$ Hz, 1H, PTzH), 7.18 (t, $J=7.2$ Hz, 1H, PTzH), 7.50 (s, 1H, =CH), 7.66 (s, 1H, PTzH), 7.80 (d, $J=7.2$ Hz, 2H, ArH $\times 2$), 7.93 (d, $J=8.0$ Hz, 1H, PTzH), 8.27 (d, $J=7.2$ Hz, 2H, ArH $\times 2$). IR (KBr, ν/cm^{-1}): 2957, 2926 (ν_{as} , CH), 2856 (ν_{s} , CH), 2210 (CN), 1585, 1566, 1518, 1497 (benzene ring), 1460 (CH_2), 1338 (CHR_3), 1205 (C–N), 852 (p -disubstitution on the benzene ring).

Compound 3c: Rf value: 0.53 (chloroform). Compound **3c** was obtained as a wine-colored powder in 58.9% yield. FAB-MS: $m/z=441.1$ $[M]^+$. UV-vis (THF): $\lambda_{\max}=454$ nm. $^1\text{H-NMR}$ (400 MHz, Chloroform- d , δ): 0.91 (t, $J=7.2$ Hz, 3H, CH_3), 0.97 (d, $J=7.2$ Hz, 3H, CH_3), 1.24 (m, 1H, CH), 1.55 (m, 1H, CH), 2.01 (m, 1H, CH), 3.67 (p, $J=7.6$ Hz, 1H, CH), 3.82 (p, $J=6.4$ Hz, 1H, CH), 6.91 (d, $J=8.0$ Hz, 1H, PTzH), 6.93 (d, $J=8.8$ Hz, 1H, PTzH), 6.99 (t, $J=7.2$ Hz, 1H, PTzH), 7.13 (d, $J=7.2$ Hz, 1H, PTzH), 7.17 (t, $J=8.0$ Hz, 1H, PTzH), 7.49 (s, 1H, PTzH), 7.65 (s, 1H, =CH), 7.79 (d, $J=8.8$ Hz, 2H, ArH $\times 2$), 7.88 (d, $J=8.8$ Hz, 1H, PTzH), 8.26 (d, $J=8.8$ Hz, 2H, ArH $\times 2$). IR (KBr, ν/cm^{-1}): 2961, 2928 (ν_{as} , CH), 2873 (ν_{s} , CH), 2212 (CN), 1585, 1568, 1517, 1497 (benzene ring), 1462 (CH_2), 1339 (CHR_3), 1208 (C–N), 853 (p -disubstitution on the benzene ring), 751 (CH).

Compound 3d: Rf value: 0.72 (chloroform). Compound **3d** was obtained as a wine-colored powder in 57.2% yield. FAB-MS: $m/z=441.1$ $[M]^+$. UV-vis (THF): $\lambda_{\max}=454$ nm. $^1\text{H-NMR}$ (400 MHz, Chloroform- d , δ): 0.92 (t, $J=7.2$ Hz, 3H, CH_3), 0.99

(d, $J=7.2$ Hz, 3H, CH_3), 1.25 (m, 1H, CH), 1.56 (m, 1H, CH), 2.02 (m, 1H, CH), 3.66 (p, $J=8.0$ Hz, 1H, CH), 3.85 (p, $J=7.2$ Hz, 1H, CH), 6.91 (d, $J=8.0$ Hz, 1H, PTzH), 6.94 (d, $J=8.8$ Hz, 1H, PTzH), 6.99 (t, $J=7.2$ Hz, 1H, PTzH), 7.17 (d, $J=7.6$ Hz, 1H, PTzH), 7.19 (t, $J=8.0$ Hz, 1H, PTzH), 7.50 (s, 1H, PTzH), 7.66 (s, 1H, =CH), 7.80 (d, $J=8.4$ Hz, 2H, ArH $\times 2$), 7.88 (d, $J=8.8$ Hz, 1H, PTzH), 8.29 (d, $J=8.8$ Hz, 2H, ArH $\times 2$). IR (KBr, ν/cm^{-1}): 2959, 2926 (ν_{as} , CH), 2855 (ν_{s} , CH), 2210 (CN), 1585, 1566, 1518, 1499 (benzene ring), 1462 (CH_2), 1340 (CHR_3), 1207 (C–N), 853 (p -disubstitution on the benzene ring), 750 (CH).

2.4. Device fabrication

The photorefractive composite film was fabricated by solution-casting approach. Firstly, organic photorefractive molecular glasses and photoconductive polymer (PVK) were respectively dissolved in THF at a concentration of 5 mg/ml. The photosensitizer (TNFM) was also prepared as a THF solution with a concentration of 1 mg/ml. Afterwards, the solutions of organic photorefractive molecular glasses, PVK and TNFM were mixed accordingly to a certain volume proportion and filtered by a PTEF filter with a pore size of 0.2 μm . After a majority of solvent was evaporated, the solution was added dropwise to the ITO substrate, which was heated to 40 $^\circ\text{C}$ with a digital hot plate in order to speed up the solvent evaporation under good ventilation. Subsequently, the solid sample was dried overnight in vacuum in order to remove the residual solvent. After that, another piece of ITO glass was covered on the solid sample at 70 $^\circ\text{C}$, where the potential crystal would be eliminated. The photorefractive composite film was immediately pressed while the film thickness was controlled through a spacer of 100 μm . Finally, the device was suddenly cooled down in order to keep the photorefractive composite film in a good amorphous state. The fabricated devices were kept in the refrigerator for photorefractive characterization.

2.5. Photorefractive characterization

The photorefractive device was characterized with an experimental setup as in Fig. 1. A tilted grating is written inside the photorefractive devices at an oblique incidence angle. Two equal p -polarized beams (beams 1 and 2) with a wavelength of $\lambda=780$ nm and the intensity of 9.0 mW, which are obtained by a nonpolarized beam splitter, are crossed inside the device at external incidence angles of 30 $^\circ$ and 60 $^\circ$, respectively. The photocurrent and the photorefractive property are measured under the external electric field. First of all, the dark current (I_d) is monitored by measuring the current on a series-connected resistance of $4.7 \times 10^6 \Omega$ without any illumination. Then, the current under illumination (I_i) is measured by the same approach

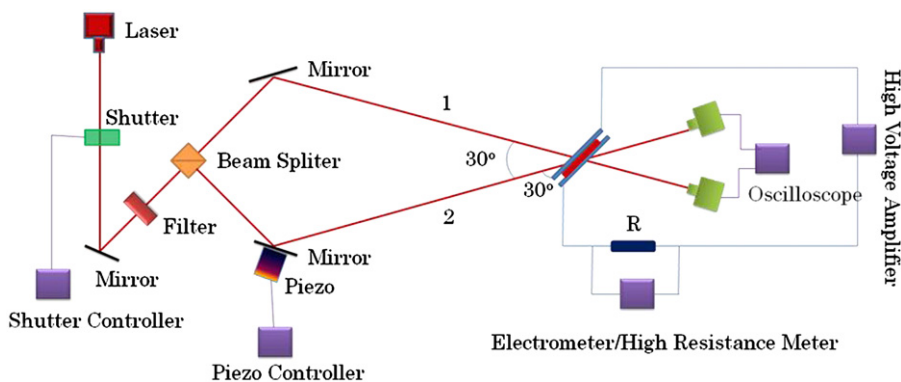


Fig. 1. Optical setup for photorefractive characterization.

only when beam 1 is applied. Finally, the photocurrent (I_p) is calculated by the formula $I_p = I_i - I_d$. The photorefractive property was investigated by the measurement of steady two beam coupling (TBC). When the electric field is switched on and the energy transfer between both beams reaches a stable state, one beam is moved at a constant speed by a piezomirror under the control of piezodriver and function generator. The total power of modulated transmitted signals is monitored by identical photo-detectors and recorded by a digital oscilloscope.

3. Results and discussion

3.1. Molecular design

The photorefractive chromophore is first designed on the basis of the general molecular design principle of nonlinear chromophore, that the nonlinear optical molecules are based upon aromatic π -electron systems asymmetrically end-capped with electron donating and accepting groups [44–47]. Herein, the excellent electron-donating ability of phenothiazine in the photorefractive chromophore provides the near-infrared response probability of the photorefractive devices. Both nitril and cyano act as acceptors. The specific molecular structure was illustrated in Fig. 2 (left). Besides, the aliphatic chains with a linear, racemic/homochiral asymmetrically branched chemical structure as shown in Fig. 2 (right) are introduced into the photorefractive chromophore as an auxiliary group, which will induce different molecular states, such as crystalline or glassy state. It was well known that there is a stereogenic center in the asymmetrically branched aliphatic chain, i.e., a stereogenic carbon, which has four different substituents. If these four different substituents are arranged around the stereogenic carbon in different orders such as clockwise or counterclockwise, *R*- or *S*-enantiomer with

different absolute configurations would be obtained. The *R*- or *S*-enantiomer oppositely interacts with the light in different absorption efficiencies, which might result in different photorefractive performances. In order to investigate the effect of chiral difference on the molecular state and the photorefractive property, the racemic and homochiral asymmetrically branched aliphatic chains with the same chemical structure are also linked with the phenothiazine-based photorefractive chromophore. The specific synthetic route of all the phenothiazine-based compounds was shown in Scheme 1. The chemical structures of all the compounds, which were characterized by $^1\text{H-NMR}$, IR and FAB-MS, are in accord with the chemical structure in Scheme 1.

3.2. Absorption property

The absorption property of photorefractive compounds **3a**, **3b**, **3c**, **3d** was characterized by the measurement of UV–vis spectra in the THF dilute solution with a concentration of 1.14×10^{-5} mol/l, as shown in Fig. 3(a). The result indicated that all the compounds have two absorption peaks within the visible region. One is located at 321 nm and the other, i.e., the absorption maximum wavelength, at 458 nm for compound **3a**, 456 nm for compound **3b**, 454 nm for compound **3c**, 454 nm for compound **3d** respectively. Simultaneously, the relationship between the absorbance and the solution concentration was measured at the absorption maximum wavelength of compounds **3a**, **3b**, **3c**, **3d** using the THF solutions with different concentrations as plotted in Fig. 3(b). Obviously, the absorbance of all the compounds takes on a linearly monotonous increment with the increase of solution concentration. Sequentially, the molar absorption coefficient at the absorption maximum wavelength was calculated with the formula $\epsilon = A/bc$. Here, ϵ is the molar absorption coefficient, A is the absorbance at the absorption maximum, b is the cuvette

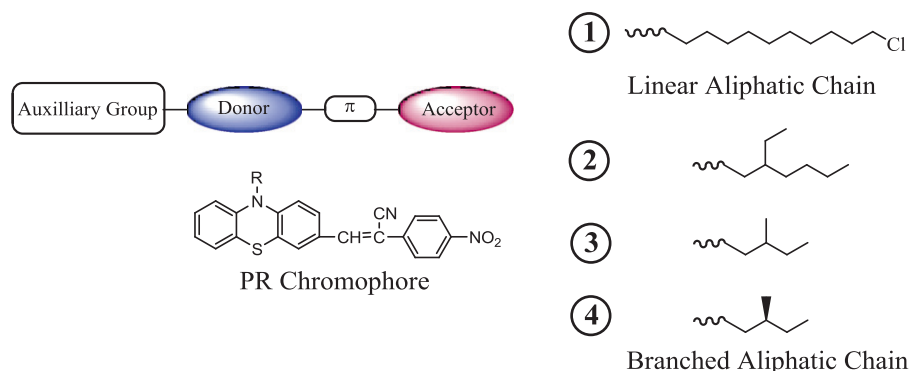


Fig. 2. Molecular design of organic near-infrared phenothiazine-based photorefractive compounds.

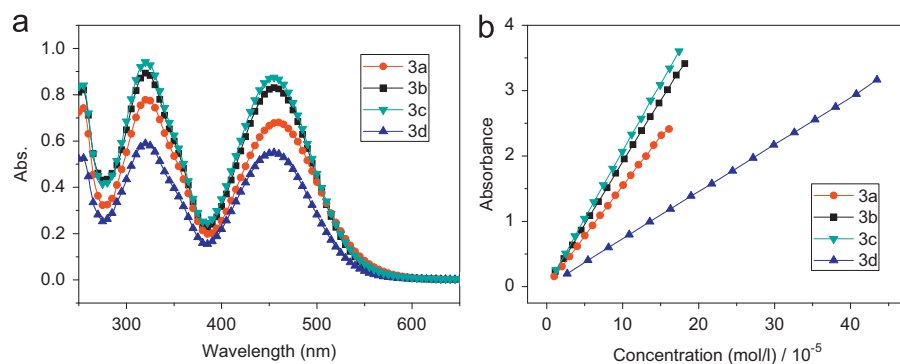


Fig. 3. UV–vis spectra of phenothiazine-based compounds (a) ($c = 1.14 \times 10^{-5}$ mol/l) and the relationship of absorbance versus concentration at the absorption maximum wavelength (b).

thickness, and c is the molar concentration. The calculation results suggested that the molar absorption coefficients of compounds **3a**, **3b**, **3c**, **3d** are 5.96×10^4 l/mol cm, 7.28×10^4 l/mol cm, 7.68×10^4 l/mol cm, 4.82×10^4 l/mol cm respectively. Evidently, the molar absorption coefficient of compound **3d** with a homochiral asymmetrically branched aliphatic chain, (S)-(+)-2-methylbutyl group, is less than compound **3a** with a linear aliphatic chain, 10-chlorooctyl group and compounds **3b/3c** with racemic asymmetrically branched aliphatic chain, 2-ethylhexyl/2-methylbutyl group. The absorbance-versus-concentration plot in Fig. 3(b) also showed that the absorbance of compound **3d**, at every concentration is clearly less than that of other compounds. Whereas, the absorbance-versus-concentration curves of other compounds are very close, especially compounds **3b** and **3c**, because they both have a racemic asymmetrically branched aliphatic chain. Therefore, we draw a conclusion that the homochiral asymmetrically branched aliphatic chain, (S)-(+)-2-methylbutyl group, has a hypochromic effect. In other words, the linear aliphatic chain, 10-chlorooctyl group, and the racemic asymmetrically branched aliphatic chain, 2-ethylhexyl/2-methylbutyl group, has a hyperchromic effect. This probably resulted from the enantiomers' absorption of left- and right-circularly polarized light to different degrees, which are included in the light source of the spectrophotometer.

3.3. Thermal property

The thermal property of photorefractive compounds **3a**, **3b**, **3c**, **3d** was investigated by the TG measurement under the nitrogen atmosphere at a heating rate of $10^\circ\text{C}/\text{min}$. The TG and DTG curves were illustrated in Fig. 4. The TG and DTG curves of compound **3a** with a linear aliphatic chain, 10-chlorooctyl group, have an evident difference from compounds **3b**, **3c**, **3d** with asymmetrically branched aliphatic chains, regardless of the racemic or the homochiral group. The degradation temperature of 283°C for compound **3a**, which is defined as the temperature at the loss-weight of 5% on the TG curve, is less than 324°C for compound **3b**, 307°C for compound **3c**, 310°C for compound **3d**. The degradation peak temperature of 300°C on the DTG curve of compound **3a** is also less than the compounds **3b**, **3c**, **3d**, which have the same degradation peak temperature of 354°C . The degradation peak height of $16.9 \mu\text{V}/\text{mg}$ on the DTG curve of compound **3a** is obviously higher than $4.8 \mu\text{V}/\text{mg}$ for compound **3b**, $5.7 \mu\text{V}/\text{mg}$ for compound **3c**, $4.8 \mu\text{V}/\text{mg}$ for compound **3d**. The full width at half a maximum of 7°C for the degradation peak of compound **3a** on the DTG curve is also a lot evidently narrower than 22°C for compound **3b**, 24°C for compound **3c**, 24°C for

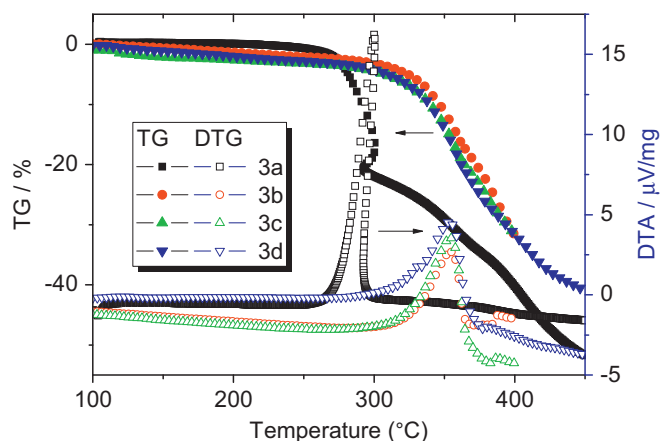


Fig. 4. TG and DTG curves of phenothiazine-based compounds.

compound **3d**. All those results showed that compound **3a** with a linear aliphatic chain degrades more easily and faster than compounds **3b**, **3c**, **3d** with asymmetrically branched aliphatic chains. Even, this fast decomposition causes a temporal temperature withdrawal on the TG curve of compound **3a**. Therefore, we came to a conclusion that the introduction of asymmetrically branched aliphatic chain enhances the thermal performance, independent of racemic or homochiral group. Finally, it was noted that the loss-weight ratio of compounds **3a**, **3b**, **3c**, **3d** at the degradation peak, which is 22.0%, 12.8%, 15.3% and 15.8%, respectively is not more than the weight content of aliphatic chain in the compounds, which is 32.1%, 23.4%, 16.1% and 16.1% respectively. This indicates that the degradation at the degradation peak comes mainly from the decomposition of aliphatic chains.

3.4. DSC measurement

All the photorefractive compounds **3a**, **3b**, **3c**, **3d** were also characterized by the DSC measurement under the nitrogen atmosphere at a scanning rate of $10^\circ\text{C}/\text{min}$. In order to study the effect of chemical structure of aliphatic chains on the phase state of photorefractive compounds in detail, the DSC curves were measured from -40°C to the degradation temperature through the first heating of powder samples, the cooling, and the second heating with the same programmed temperature controlling, as shown in Fig. 5. The results indicated that compound **3a** with a linear aliphatic chain is a crystalline compound. Its melting points at the first and second heating processes are 107.4°C and 107.0°C respectively. The freezing point in the cooling process is 92.4°C , which is a little less than the melting points. At the same time, the enthalpy change at the first heating, cooling, second heating processes are 35.5 J/g , 37.0 J/g and 35.3 J/g respectively. However, when the linear aliphatic chain is substituted by the asymmetrically branched aliphatic chains including racemic and homochiral asymmetrically branched aliphatic chains, crystalline compound **3a** is turned into glassy compounds **3b**, **3c** and **3d**, i.e., organic molecular glasses, which is obviously proved by the DSC curves in Fig. 5, especially the second-heating curves with the same heat history. Together with the TG result that the thermal performance is enhanced by the introduction of asymmetrically branched aliphatic chains including racemic and homochiral groups, it was suggested that glassy compounds **3b**, **3c** and **3d** are more thermally stable than crystalline compound **3a**.

The racemic asymmetrical branched aliphatic chain, 2-ethylhexyl group, which is often used in the course of the synthesis of organic optoelectronic materials in order to increase the solubility and film-processing ability, is first introduced into the photorefractive chromophore in place of the linear aliphatic chain, 10-chlorooctyl group in compound **3a**. In consequence, organic molecular glass, compound **3b**, is obtained whose glass transition temperature is 21.1°C at the first heating, 9.0°C at the cooling and 16.6°C at the second heating, as shown in Fig. 5. Notably, there is a very small melting point at 65.1°C with an enthalpy change of 0.25 J/g in the first-heating DSC curve of compound **3b**, indicative of a weak crystallization tendency. However, this tiny melting point will disappear by heating the sample over the melting point, as shown in the second-heating DSC curve of compound **3b** in Fig. 4. This means that the weak crystallization tendency does not affect the achievement of organic glassy state as long as the sample is heated over the melting point. In order to study the volume effect of branched aliphatic chain on the probability to achieve organic molecular glasses, the smaller racemic asymmetrical branched aliphatic chain, 2-methylbutyl group, is introduced into the photorefractive chromophore to take the place of 2-ethylhexyl group in compound **3b**. Although there is only one melting point at 57.1°C to appear in the first-heating

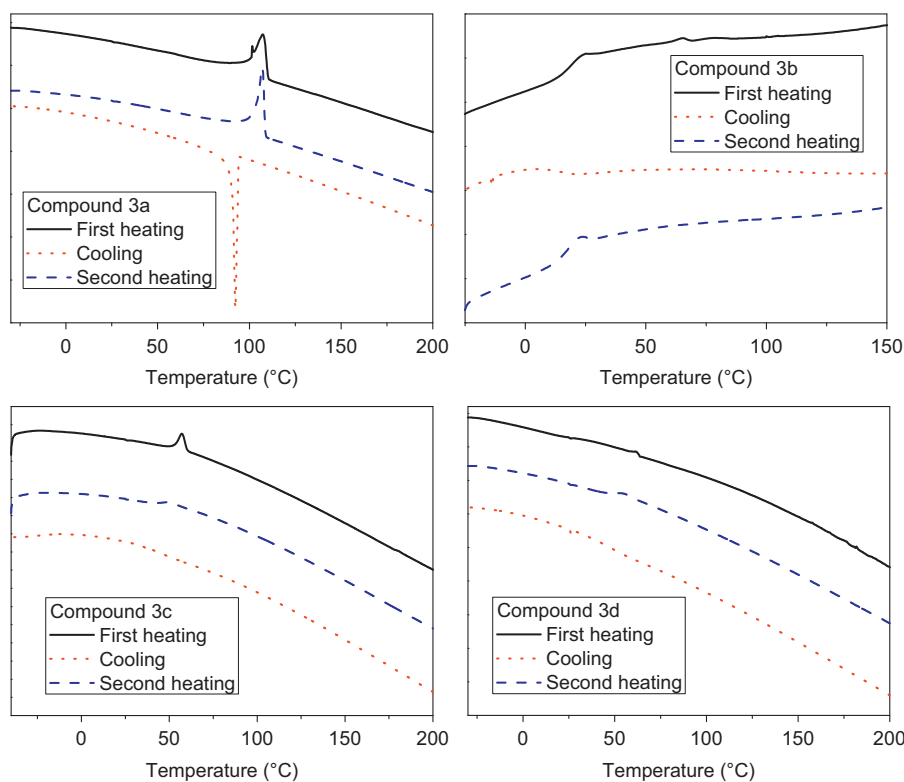


Fig. 5. DSC curves of phenothiazine-based compounds.

DSC curve of compound **3c**, its enthalpy change of 6.9 J/g is much less than 35.5 J/g of compound **3a** at the first heating. This indicated that the introduction of 2-methylbutyl group decreases the molecular degree of order of compound **3c** to a large extent compared with compound **3a**. Like the small melting point in the first-heating DSC curve of compound **3b**, the melting point of compound **3c** at the first heating will also disappear at the cooling and second-heating processes. The appearance of glass transition at 46.6 °C in the second-heating DSC curve of compound **3c** suggested that 2-methylbutyl group is potentially the smallest racemic asymmetrically branched aliphatic chain to synthesize organic molecular glass for the present photorefractive chromophore. Finally, the homochiral asymmetrically branched aliphatic chain, (*S*)-(+)-2-methylbutyl group, which has the same chemical conformation as 2-methylbutyl group in compound **3c**, is also connected with the photorefractive chromophore in order to understand if the introduction of homochiral asymmetrically branched aliphatic chain may result in organic molecular glass. The result is similar to the introduction of 2-ethylhexyl group into compound **3b**. The glass transition temperatures of 28.2 °C at the first heating, 45.4 °C at the cooling and 49.1 °C at the second heating in the DSC curves of compound **3d** in Fig. 4 indicated that the introduction of homochiral asymmetrically branched aliphatic chain can still lead to the achievement of organic molecular glass. Similarly to compound **3b**, the small melting point with an enthalpy change of 0.36 J/g disappears at the cooling and second-heating processes. Additionally, the glass transition temperatures of compounds **3b**, **3c** and **3d** at the second-heating (16.6 °C, 46.6 °C and 49.1 °C), which come from the samples with the same heat history, suggested that the glass transition temperature of compound **3b** with a large-volume asymmetrically branched aliphatic chain is less than compounds **3c** and **3d** with a small-volume asymmetrically branched aliphatic chain, independent of racemic or homochiral group. Simultaneously, the glass transition temperature of compound **3d** with homochiral asymmetrically

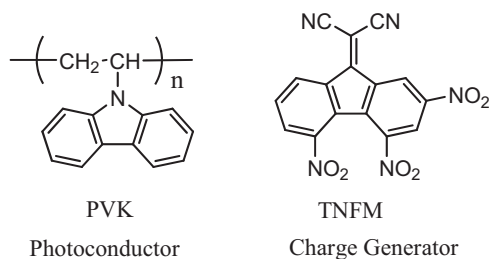


Fig. 6. Chemical structures of photoconductive polymer (PVK) and charge generator (TNFM).

branched aliphatic chain is a little more than compound **3c** with racemic asymmetrically branched aliphatic chain. This is on account of the same chemical conformation but different molecular configuration.

3.5. Photorefractive property

Compounds **3c** and **3d** with the same chemical conformation are selected as organic photorefractive molecular glasses for the photorefractive measurement in order to investigate the effect of racemic and homochiral asymmetrically branched aliphatic chains on the photorefractive property. Poly(*N*-vinylcarbazole) (PVK) is used as a photoconductive polymer and (2,4,7-trinitro-9-fluorenylidene) malononitrile (TNFM) as a photosensitizer. Their chemical structures were illustrated in Fig. 6. The GPC measurement indicated that the number average molecular weight, weight average molecular weight and polydispersity of PVK are 2.49×10^5 , 1.70×10^6 and 6.86 respectively. In this work, four photorefractive devices, whose thicknesses were controlled by the spacer of 100 μm, were prepared by the fabrication approach depicted in

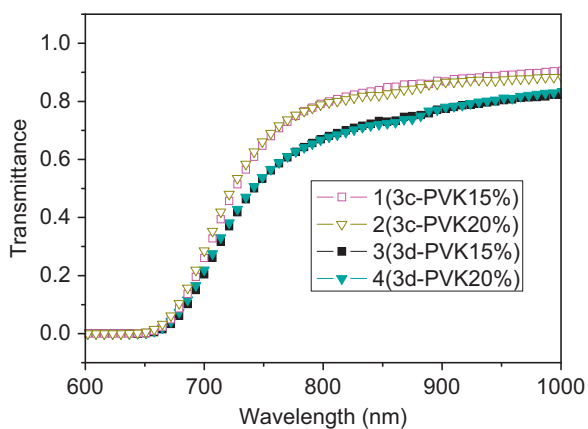


Fig. 7. Transmittance spectra of all the photorefractive devices.

Section 2. The device configuration and composite component were shown as follows:

1. ITO/compound **3c** (84%)/TNFM (1.0%)/PVK (15%)/ITO
2. ITO/compound **3c** (79%)/TNFM (1.0%)/PVK (20%)/ITO
3. ITO/compound **3d** (84%)/TNFM (1.0%)/PVK (15%)/ITO
4. ITO/compound **3d** (79%)/TNFM (1.0%)/PVK (20%)/ITO

The transmittance spectra of the photorefractive devices were measured as shown in Fig. 7. The results indicated that all the photorefractive devices have a good transmittance property at more than 700 nm, which basically belongs to the near-infrared region. In addition, at 780 nm where the photorefractive property will be investigated, compound **3c** has a better transmittance property than compound **3d** in solid film, which resulted from the high transmittances of 75.7% for device 1, 75.9% for device 2 and the low transmittances of 63.4% for device 3, 63.3% for device 4. In other words, compound **3d** has a better absorption property than compound **3c** in solid film. This is proved by the low absorption coefficients of 27.8 cm^{-1} in device 1, 27.6 cm^{-1} for device 2 and the high absorption coefficient of 45.6 cm^{-1} for device 3, 45.7 cm^{-1} for device 4, which were calculated by the formula: $I/I_0 = e^{-\alpha L}$. This result is completely contrary to the fact that the molar absorption coefficient of compound **3d** in the dilute solution is less than that of the compound **3c**. This is induced by different molecular states, i.e., the single molecular state in the dilute solution and the condensed state in solid film. The small transmittance or the large absorption coefficients of devices 3 and 4 of compound **3d** is caused by the low steric hindrance of homochiral asymmetrically branched aliphatic group (here, S-enantiomer). It was well known that the low steric hindrance results in the better intermolecular interaction of donor–acceptor dipole compounds. Consequently, the exciplex will be formed more easily, which is an excited donor–acceptor complex and dissociated in the ground state. Therefore, the small transmittance or the large absorption coefficient can be obtained in solid film of homochiral compound **3d**. In contrast, the different responses of the enantiomers to left- and right-circularly polarized lights does not appear in solid film. At the same time, we noted that the content difference of PVK induces only a little change of the glass transition temperature as shown in Table 1. All the data of the transmittance, the absorption coefficient in solid film and the glass transition temperature of the composites were listed in Table 1.

The photocurrent of all the photorefractive devices was tested by the measurement approach described in Section 2. The photocurrent-versus-voltage curves were shown in Fig. 8. It was obvious that the photocurrent of device 1 from compound **3c** is

Table 1
Data of all the photorefractive devices at 780 nm^a.

Devices	$T_g / ^\circ\text{C}$	Transmittance / %	α / cm^{-1}	Γ / cm^{-1}	n_{1s}
1	8.1	75.7	27.8	11.8	1.42×10^{-4}
2	7.6	75.9	27.6	17.6	2.11×10^{-4}
3	5.5	63.4	45.6	7.4	0.88×10^{-4}
4	3.2	63.3	45.7	12.4	1.49×10^{-4}

^a T_g is the glass transition temperature of the composite, α is the absorption coefficient in solid film calculated with the formula $I/I_0 = e^{-\alpha L}$, Γ is the modulated amplitude of the coupling constant at 780 nm and 1.5 kV, and n_1 is the modulated amplitude of the refractive index at 780 nm and 1.5 kV.

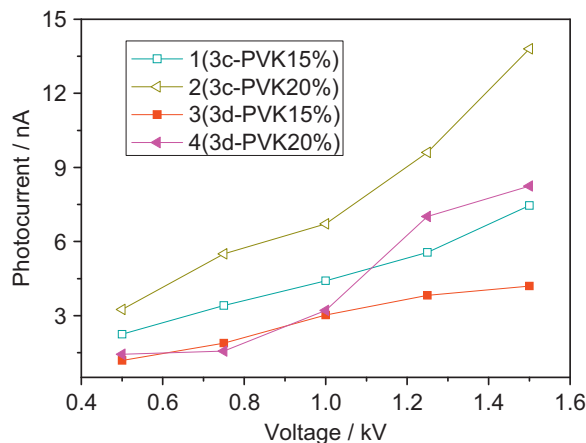


Fig. 8. Photocurrent-versus-voltage curves of all the photorefractive devices.

larger than device 3 from compound **3d** when the PVK content is 15% and the photocurrent of device 2 from compound **3c** is also larger than device 4 from compound **3d** when the PVK content is 20%. This result indicated that compound **3c** with racemic asymmetrically branched chain has a higher optical charge generation quantum efficiency in solid film than the compound **3d** with homochiral asymmetrically branched chain. Evidently, the high absorption coefficient of compound **3d** in solid film does not cause the high photocurrent. Contrarily, the homochiral asymmetrically branched aliphatic chain in compound **3d** leads to the low optical charge generation quantum efficiency and then the low photocurrent in the photorefractive device. The racemic asymmetrically branched aliphatic chain in compound **3c** causes the high optical charge generation quantum efficiency and then the high photocurrent in the photorefractive device. We assumed that this result should be derived from the formation of different exciplexes such as racemic and homochiral charge-transfer complexes, which play a photosensitizer role in photorefractive effect. In other words, racemic charge-transfer complex might induce high optical charge generation quantum efficiency and homochiral charge-transfer complex might induce low optical charge generation quantum efficiency. This point needs to be further investigated in detail although chiral charge-transfer complexes have been investigated [41–42]. Besides, it was also noted from the photocurrent curves in Fig. 8 that the high content of photoconductive polymer PVK results in the high photocurrent.

The photorefractive property was investigated by the measurement of steady two beam coupling, which was described in Section 2. The total powers of modulated transmitted signals are measured with one beam moved at a constant speed by a piezoelectric stage driven by a piezo driver and a function generator after the energy transfer between both beams reaches a steady state. The transmitted powers for beams 1 and 2 of

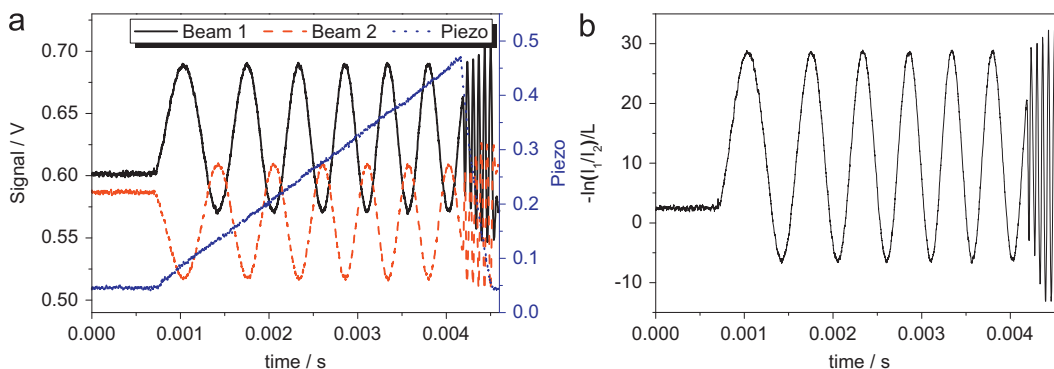


Fig. 9. Transmitted power for beams 1 and 2 of device 2 together with piezoelectric function signal as the piezomirror is translated with a piezoelectric stage driven by a piezodriver and a function generator (a) and the modulated curve of the coupling constant (b) at 1.5 kV.

device 2 at 1.5 kV together with piezoelectric function signal were illustrated in Fig. 9a. Both beams are evidently diffracted by the grating in existence after the mirror is translated. Generally, the intensities $I_1(z)$ and $I_2(z)$ are given as formula (1) and (2) [48]:

$$I_1(z) = I_1(0) \frac{1+m^{-1}}{1+m^{-1}e^{-\gamma z}} e^{-\alpha z} \quad (1)$$

$$I_2(z) = I_2(0) \frac{1+m}{1+me^{-\gamma z}} e^{-\alpha z} \quad (2)$$

Here, γ is the coupling constant, z is any position inside the photorefractive device, α is the absorption coefficient, and m is the input intensity ratio:

$$m = \frac{I_1(0)}{I_2(0)} \quad (3)$$

In our case, the thickness is L (100 μm) and $I_1(0)$ is equal to $I_2(0)$, namely, $m=1$. Therefore,

$$\frac{I_1(L)}{I_2(L)} = me^{-\gamma L} = e^{-\gamma L} \quad (4)$$

Simultaneously,

$$\gamma = \frac{2\pi n_1}{\lambda \cos \theta} \sin \phi \quad (5)$$

Here, n_1 is the modulated amplitude of refractive index, λ is the laser wavelength; 2θ is the angle between the beams inside the medium, and ϕ is the phase shift between index grating and light interference pattern. Finally, we can know that the coupling constant can be shown as follows:

$$\gamma = -\frac{1}{L} \ln \frac{I_1(L)}{I_2(L)} = \frac{2\pi n_1}{\lambda \cos \theta} \sin \phi \quad (6)$$

Here, in order to evaluate the photorefractive property, we define the modulated amplitude of the coupling constant Γ as below:

$$\Gamma = \frac{2\pi n_1}{\lambda \cos \theta} \quad (7)$$

The modulated curve of the coupling constant of device 2 at 1.5 kV was given as an example in Fig. 9b, which is calculated with a formula $\gamma = -(1/L)\ln(I_1(L)/I_2(L))$. At this time, the Γ value is equal to 17.6 cm^{-1} . The modulated amplitude of the refractive index is also calculated as 2.11×10^{-4} with the above definition formula (7). All the data of Γ and the modulated amplitude of the refractive index at 780 nm and 1.5 kV were summarized and listed in Table 1.

The modulated amplitude of the coupling constant Γ at different operating voltages of all the photorefractive devices was plotted in Fig. 10. Evidently, the Γ value of device 1 from compound **3c** is larger than device 3 from compound **3d** when the

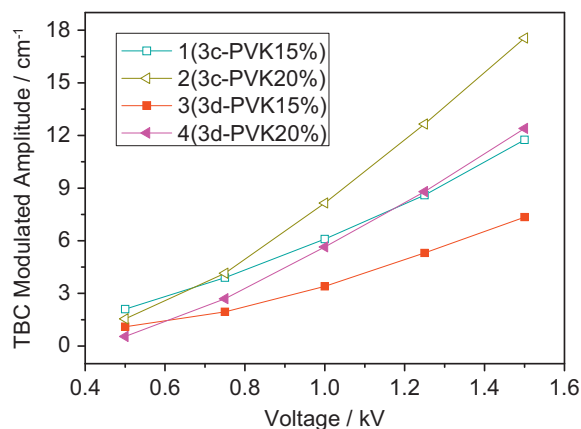


Fig. 10. Modulated amplitude of the coupling constant in all the photorefractive devices at different operating voltages.

PVK content is 15%. The Γ value of device 2 from compound **3c** is also larger than device 4 from compound **3d** when the PVK content is 20%. This result suggested that the coupling constant of compound **3c** with racemic asymmetrically branched aliphatic chain has higher modulated amplitude than compound **3d** with homochiral asymmetrically branched aliphatic chain. The Γ value has a similar change trend to the photocurrent in Fig. 8 with the increase of applied voltages and the PVK content. The low optical charge generation quantum efficiency from homochiral asymmetrically branched aliphatic chain in compound **3d** not only results in the low photocurrent but also the low Γ value. Vice versa, the high optical charge generation quantum efficiency from racemic asymmetrically branched aliphatic chain in compound **3c** causes the high photocurrent and finally the high Γ value. This is in accordance with the common principle in the photorefractive materials that the photorefractive performance is proportional to the photocurrent. Therefore, we deemed that the flexible homochiral asymmetrically branched aliphatic chain cannot make rigid photorefractive chromophore much more ordered, which will be one necessary condition to improve the photorefractive performance. The racemic group is more beneficial to the improvement of photorefractive performance than the homochiral.

4. Conclusions

Organic near-infrared photorefractive molecular glasses with a phenothiazine moiety were designed and synthesized through the introduction of linear, racemic/homochiral asymmetrically

branched aliphatic chains into photorefractive chromophore as an auxiliary group. All the compounds were characterized with ¹H-NMR, IR, FAB-MS, UV-vis, TG, DSC, etc. The results indicated that all the compounds are in accordance with the chemical structures in Scheme 1. The effect of different aliphatic chains on absorption and thermal properties was investigated in detail. The UV-vis measurement suggested that the homochiral asymmetrically branched aliphatic chain has a strong hypochromic effect in the dilute solution. The DSC measurement told us that the introduction of asymmetrically branched aliphatic chains is the key issue to synthesize organic molecular glasses whether it is racemic or homochiral. The effect of racemic/homochiral asymmetrically branched aliphatic group on photorefractive performance was measured carefully with PVK as a photoconductive polymer and with TNFM as a photosensitizer. The results indicated that the homochiral asymmetrically branched aliphatic chain results in the low optical charge generation quantum efficiency and then the low photocurrent in the photorefractive devices, which finally causes the low modulated amplitude of the coupling constant. Contrarily, the high optical charge generation quantum efficiency from the racemic asymmetrically branched aliphatic chain leads to the high photocurrent and finally the high modulated amplitude of the coupling constant. Therefore, the racemic asymmetrically branched aliphatic group is more of benefit to photorefractive performance than homochiral asymmetrically branched aliphatic group when the homochiral group cannot make rigid photorefractive chromophore much more ordered.

Acknowledgment

The authors greatly acknowledge the support from the Japan Society for the Promotion of Science (JSPS). Simultaneously, we also thank Prof. Koji Araki and Mr. Isao Yoshikawa in Institute of Industrial Science, the University of Tokyo for their help in the measurements of IR spectra, FAB-MS spectra, TG and DSC.

References

- [1] C.S. Choi, I.K. Moon, N. Kim, Appl. Phys. Lett. 94 (2009) 053302.
- [2] J. Hwang, J. Seo, J. Sohn, S.Y. Park, Opt. Mater. 21 (2003) 359–364.
- [3] H. Chun, N.J. Kim, W.J. Joo, J.W. Han, H.O. Chang, N. Kim, Synth. Met. 129 (2002) 281–283.
- [4] U. Gubler, M. He, D. Wright, Y. Roh, R. Twieg, W.E. Moerner, Adv. Mater. 14 (2002) 313–317.
- [5] J. Sohn, J. Hwang, S.Y. Park, G.J. Lee, Jpn. J. Appl. Phys., 40 (2001) 3301–3304.
- [6] S. Tang, M.R. Liu, P. Lu, H. Xia, M. Li, Z.Q. Xie, F.Z. Shen, C. Gu, H.P. Wang, B. Yang, Y.G. Ma, Adv. Funct. Mater. 17 (2007) 2869–2877.
- [7] L.H. Chan, R.H. Lee, C.F. Hsieh, H.C. Yeh, C.T. Chen, J. Am. Chem. Soc. 124 (2002) 6469–6479.
- [8] D.F. O'Brien, P.E. Burrows, S.R. Forrest, B.E. Koene, D.E. Loy, M.E. Thompson, Adv. Mater. 10 (1998) 1108–1112.
- [9] M.R. Robinson, S.J. Wang, A.J. Heeger, G.C. Bazan, Adv. Funct. Mater. 11 (2001) 413–419.
- [10] H. Kageyama, H. Ohishi, M. Janaka, Y. Ohmori, Y. Shirota, Adv. Funct. Mater. 19 (2009), 3948–2955.
- [11] H. Kageyama, H. Ohishi, M. Tanaka, Y. Ohmori, Y. Shirota, Appl. Phys. Lett. 94 (2009) 063304.
- [12] R. Schroeder, L.A. Majewski, M. Grell, Adv. Mater. 16 (2004) 633–636+576.
- [13] M. Halik, H. Klauk, U. Zschieschang, G. Schmid, C. Dehm, M. Schutz, S. Malsch, F. Effenberger, M. Brunnbauer, F. Stellacci, Nature 431 (2004) 963–966.
- [14] P.M. Lundquist, R. Wortmann, C. Geletneky, R.J. Twieg, M. Jurich, V.Y. Lee, C.R. Moylan, D.M. Burland, Science 274 (1996) 1182–1185.
- [15] S.J. Zilker, U. Hofmann, Appl. Opt. 39 (2000) 2287–2290.
- [16] S. Schloter, A. Schreiber, M. Grasmuck, A. Leopold, M. Kol'chenko, J. Pan, C. Hohle, P. Stroehriegel, S.J. Zilker, D. Haarer, Appl. Phys. B: Lasers Opt. 68 (1999) 899–906.
- [17] Q. Wang, N. Quevada, A. Gharavi, L.P. Yu, ACS Symp. Ser. 726 (1999) 226–236.
- [18] F. Fan, J.S. Liu, Y. Zhang, Y. Chen, J. Mod. Opt. 56 (2009) 1392–1395.
- [19] M. Asaro, M. Sheldon, Z.G. Chen, O. Ostroverkhova, W.E. Moerner, Opt. Lett. 30 (2005) 519–521.
- [20] Z. Chen, M. Asaro, O. Ostroverkhova, W.E. Moerner, M. He, R.J. Twieg, Opt. Lett. 28 (2003) 2509–2511.
- [21] U. Hofmann, M. Grasmuck, A. Leopold, A. Schreiber, S. Schloter, C. Hohle, P. Stroehriegel, D. Haarer, S.J. Zilker, J. Phys. Chem. B 104 (2000) 3887–3891.
- [22] S.J. Zilker, M. Grasmuck, J. Wolff, S. Schloter, A. Leopold, M.A. Kol'chenko, U. Hofmann, A. Schreiber, P. Stroehriegel, C. Hohle, D. Haarer, Chem. Phys. Lett. 306 (1999) 285–290.
- [23] M. Grasmuck, A. Schreiber, U. Hofmann, S.J. Zilker, A. Leopold, S. Schloter, C. Hohle, P. Stroehriegel, D. Haarer, Phys. Rev. B (Condens. Matter) 60 (1999) 16543–16548.
- [24] O. Ostroverkhova, W.E. Moerner, M. He, R.J. Twieg, Appl. Phys. Lett. 82 (2003) 3602–3604.
- [25] M. Miyasaka, A. Rajca, M. Pink, S. Rajca, Chem.–Eur. J. 10 (2004) 6531–6539.
- [26] M.H. Levi, S.J. Garth, Annu. Rev. Phys. Chem. 60 (2009) 345–365.
- [27] K. Sreekumar, D. Davis, S.K. Pati, Synth. Met. 155 (2005) 384–388.
- [28] S. Sioncke, T. Verbiest, A. Persoons, Mater. Sci. Eng. R: Rep. R42 (2003) 115–155.
- [29] B.J. Coe, E.C. Harper, K. Clays, E. Franz, Dyes Pigm. 87 (2010) 22–29.
- [30] M. Kauranen, T. Verbiest, A. Persoons, J. Nonlinear Opt. Phys. Mater. 8 (1999) 171–189.
- [31] A. Persoons, M. Kauranen, S. Van Elshocht, T. Verbiest, L. Ma, L. Pu, B.M.W. Langeveld-Voss, E.W. Meijer, Mol. Cryst. Liq. Cryst. Technol. Sect. A: Mol./Cryst./Liq. Cryst. 314 (1998) 395/93–400/98.
- [32] M. Kauranen, T. Verbiest, S. Van Elshocht, A. Persoons, Opt. Mater. 9 (1998) 286–294.
- [33] T. Verbiest, S.V. Van Elshocht, M. Kauranen, L. Hellemans, J. Snauwaert, C. Nuckolls, T.J. Katz, A. Persoons, Science 282 (1998) 913–915.
- [34] M. Kauranen, T. Verbiest, E.W. Meijer, E.E. Havinga, M.N. Teerenstra, A.J. Schouten, R.J.M. Nolte, A. Persoons, Adv. Mater. 7 (1995) 641–644.
- [35] C. Dhenaut, I. Ledoux, I.D.W. Samuel, J. Zyss, M. Bourgault, H. Le Bozec, Nature 374 (1995) 339–342.
- [36] M. Talarico, R. Termine, P. Prus, G. Barberio, D. Pucci, M. Ghedini, A. Golemme, Mol. Cryst. Liq. Cryst. 429 (2005) 65–76.
- [37] R. Termine, A. Golemme, J. Phys. Chem. B 106 (2002) 4105–4111.
- [38] R. Termine, A. Golemme, Opt. Lett. 26 (2001) 1001–1003.
- [39] R. Termine, B.C. De Simone, A. Golemme, Appl. Phys. Lett. 78 (2001) 688–690.
- [40] M.C. Guo, Z.D. Xu, X.Q. Wang, Opt. Mater. 31 (2008) 412–417.
- [41] Y. Imai, K. Kamon, S. Kido, T. Harada, N. Tajima, T. Sato, R. Kuroda, Y. Matsubara, Cryst. Eng. Commun. 11 (2009) 620–624.
- [42] Y. Imai, T. Kinuta, T. Sato, N. Tajima, R. Kuroda, Y. Matsubara, Z. Yoshida, Tetrahedron Lett. 47 (2006) 3603–3606.
- [43] M. Frantisek, B. Geraldine, G.A. Emanuel, J. Chromatogr. A 122 (1976) 205–221.
- [44] G. Archetti, A. Abbotto, R. Wortmann, Chem.—A Eur. J. 12 (2006) 7151–7160.
- [45] S.J. Zilker, Angew. Chem. Int. Ed. Engl. 39 (2000) 73–87.
- [46] S.R. Marder, B. Kippelen, A.K.Y. Jen, N. Peyghambarian, Nature 388 (1997) 845–851.
- [47] B. Kippelen, F. Meyers, N. Peyghambarian, S.R. Marder, J. Am. Chem. Soc. 119 (1997) 4559.
- [48] P. Yeh, Introduction of Photorefractive Nonlinear Optics, A Wiley Interscience Publication John Wiley & Sons, Inc., 1993.